Small-signal circuit modeling for a semiconductor optical amplifier monolithically integrated with a sampled grating distributed Bragg reflector laser

Hui Lv[1, 2*], Ziqiang Li[1], Tao Yang[1], Chuyun Huang[1]

[1]School of Science, Hubei University of Technology, Wuhan, 430068, China

[2]Wuhan National Laboratory for Optoelectronics, College of Optoelectronic Science and Engineering, Huazhong University of Science and Technology, Wuhan, 430074, China

*Corresponding author: simonlv76@gmail.com

In this paper, a small-signal equivalent circuit model of a semiconductor optical amplifier (SOA) monolithically integrated with a sampled grating distributed Bragg reflector (SGDBR) laser is presented. To take into account the wavelength dependence of the circuit parameters of our model, the extraction of parameters has been performed by fitting the circuit model including parasitic effect with measured *S*-parameters of the integrated device for different operating wavelengths of the SGDBR laser. The optical frequency chirp caused by the current modulation of the SOA section has been simulated by the obtained small-signal circuit model.

Keywords: semiconductor optical amplifier, sampled grating distributed Bragg reflector laser, small-
-signal circuit model, optical frequency chirp.

1. Introduction

Semiconductor optical amplifiers (SOAs) play an important role in optical networks due to their use in a wealth of applications. With the rapid development of photonic integrated circuits (PIC) technology, an SOA can be easily monolithically integrated with a semiconductor tunable laser to achieve highly varied functions [1–3]. For this multisection device, the SOA can act as an external modulator for the laser by direct current modulation of the SOA section, which can overcome the shortages induced by the direct modulation of the laser, such as the mode hopping. The main drawback of this application is the slow modulation response of the SOA section. However, current modulation of several GHz has been demonstrated for SOA [4], so the modulation method can be used for wavelength-division multiplexing (WDM) networks when no extremely high data rate is required.

A detailed theoretical analysis of the modulation response of an SOA has been presented in [5] using a direct solution of the photon propagation equation and the carrier rate equation. This method of analysis requires complex programming and is not suited to inclusion of electrical parasitics due to the various levels of the packaging hierarchy. TUCKER and POPE [6] proposed a lumped-element circuit modeling approach to analyze semiconductor injection lasers, which is to transform the rate equations of carrier and photon density to the microwave small-signal equivalent circuit model, including the intrinsic nonlinear behavior, heterojunction *I–V* and space-charge characteristics, package and substrate parasitics. The small-signal performance of semiconductor lasers can be easily obtained from the circuit model by using general circuit simulators (such as SPICE). In this paper, we introduce the lumped-element circuit modeling approach into the analysis of SOAs. A small-signal equivalent circuit model of an SOA monolithically integrated with a sampled grating distributed Bragg reflector (SGDBR) laser is proposed based on Tucker's model. Considering the spatial variation of the photons inside the cavity of a SOA due to a nonuniform longitudinal field distribution, some corrections are introduced into the model by use of the photon propagation equation to relate the photon density at the output facet to the injected current of an SOA. Due to the wavelength tunability of the integrated SGDBR laser and the wavelength dependence of the circuit parameters of the SOA model, the parameters are extracted by fitting the circuit model including parasitic effect with the measured *S*-parameters of the integrated device for different operating wavelengths of the SGDBR laser. By using the obtained small-signal equivalent circuit model, the optical frequency chirp caused by the current modulation of the SOA section is simulated. The simulation results agree well with the measured results presented in [1].

2. Small-signal equivalent circuit model

The rate equations of the carrier and photon density of an SOA can be expressed as [6, 7]

$$\frac{\mathrm{d}N(t)}{\mathrm{d}t} = \frac{I(t)}{qV_{\mathrm{act}}} - \frac{N(t)}{\tau_n} - \Gamma a\Big(N(t) - N_{\mathrm{tr}}\Big)S(t) \tag{1}$$

$$\frac{\mathrm{d}S(t)}{\mathrm{d}t} = \left[\Gamma a\Big(N(t) - N_{\mathrm{tr}}\Big) - \frac{1}{\tau_p}\right]S(t) + \Gamma\beta\frac{N(t)}{\tau_n} + r_{\mathrm{in}} \tag{2}$$

where $N(t)$ is the carrier density, $S(t)$ is the photon density, Γ is the optical confinement factor, a is the differential gain constant, N_{tr} is the carrier density at transparency, τ_n is the carrier lifetime and τ_p is the photon lifetime, β is the fraction of spontaneous emission coupled into the signal mode, w, d, and l are the width, thickness, and length of the active layer, respectively, r_{in} is the rate of injection of photon density due to the input signal, q is the electronic charge, and I is the current injected into the active layer. When using the above rate equations to analyze the performance of an SOA as

a whole, the spatial variations of carriers and photons inside the cavity are neglected. We use the following equations to relate the variables in Eqs. (1), (2) to the corresponding z-dependent ones

$$S(t) = \frac{1}{l} \int_0^l S(z, t) dz \tag{3}$$

A classical Shockley relationship can be used to relate the carrier density $N(t)$ to the heterojunction voltage $V_j(t)$ as follows

$$N(t) = N_e \left(\exp\left(\frac{q V_j(t)}{\eta k T} \right) - 1 \right) \tag{4}$$

where N_e is the equilibrium carrier density, η is the emission coefficient of the diode, k is the Boltzmann constant, and T is the temperature of the active layer in Kelvin scale. We split the time-varying variables into dc and ac components as follows

$$I(t) = I_0 + i \exp(j\omega t) \tag{5a}$$

$$V_j(t) = V_{j0} + v_j \exp(j\omega t) \tag{5b}$$

$$N(t) = N_0 + n \exp(j\omega t) \tag{5c}$$

$$S(t) = S_0 + s \exp(j\omega t) \tag{5d}$$

With Equations (5) substituted in Eqs. (1), (2) and (4), and with the products of small-signal terms neglected, the following equations can be obtained

$$i = v_j \left(j\omega C_t + \frac{1}{R_1} \right) + i_s \tag{6}$$

$$v_j = i_s \left(j\omega L_s + R_2 + R_{in} \right) \tag{7}$$

where

$$i_s = \Gamma a q w d l \left(N_0 - N_{tr} \right) s \tag{8a}$$

$$v_j = \frac{\eta k T}{q N_0} n \tag{8b}$$

$$R_d = \frac{\tau_n \eta k T}{q^2 w d l N_0} \tag{8c}$$

$$R_1 = \frac{R_d}{1 + a\Gamma S_0 \tau_n} \tag{8d}$$

$$C_t = \frac{\tau_n}{R_d} \tag{8e}$$

$$L_s = \frac{R_d}{\Gamma^2 a(N_0 - N_{tr})(\beta + a\tau_n S_0)} \tag{8f}$$

$$R_2 = \frac{\Gamma\beta N_0}{\tau_n S_0} L_s \tag{8g}$$

$$R_{in} = \frac{r_{in}}{S_0} L_s \tag{8h}$$

The photon propagation equation of an SOA can be expressed as [5]

$$\frac{\partial S(z, t)}{\partial z} = \left[\Gamma a\big(N(z, t) - N_{tr}\big) - \alpha_i\right] S(z, t) \tag{9}$$

where α_i is the spatially-averaged loss coefficient in the active layer of the amplifier. We neglect the z-dependence of the carrier density, integrate and normalize Eq. (9) on $[0, z]$, and then solve it for the photon density at location z in terms of the photon density at the input facet of the SOA as

$$S(z, t) = S(0, t)\exp\left\{\left[\Gamma a\big(N(t) - N_{tr}\big) - \alpha_i\right]z\right\} \tag{10}$$

At the output facet of the SOA, the photon density is

$$S(l, t) = S(0, t)\exp\left\{\left[\Gamma a\big(N(t) - N_{tr}\big) - \alpha_i\right]l\right\} \tag{11}$$

Substituting Eq. (10) in Eq. (3) gives

$$S(t) = \frac{S(0, t)\left[\exp\left\{\left[\Gamma a\big(N(t) - N_{tr}\big) - \alpha_i\right]l\right\} - 1\right]}{\left[\Gamma a\big(N(t) - N_{tr}\big) - \alpha_i\right]l} \tag{12}$$

Comparing Eq. (11) with Eq. (12), we can obtain the relationship

$$S(l, t) = \left[\Gamma a\big(N(t) - N_{tr}\big) - \alpha_i\right]lS(t) + S(0, t) \tag{13}$$

We define the output photon density as

$$S(l, t) = S_0' + s' \exp(j\omega t) \tag{14}$$

Substituting Eq. (5) and Eq. (14) in Eq. (13) gives

$$s' = \left[\Gamma a\left(N_0 - N_{\mathrm{tr}}\right) - \alpha_i \right] ls + \Gamma a l S_0 n \tag{15}$$

Defining small-signal voltage v_s as

$$v_s = s' \tag{16}$$

and then substituting Eqs. (8) and (16) in Eq. (15), we can obtain

$$v_s = i_s\left(j\omega L + R\right) \tag{17}$$

where

$$L = \frac{\Gamma a l S_0 q N_0}{\eta k T} L_s \tag{18a}$$

$$R = \frac{\Gamma a(N_0 - N_{\mathrm{tr}}) - \alpha_i}{\Gamma a q w d (N_0 - N_{\mathrm{tr}})} + \frac{\Gamma a l S_0 q N_0}{\eta k T}(R_2 + R_{\mathrm{in}}) \tag{18b}$$

    The small-signal equivalent circuit model of the intrinsic part of an SOA is directly derived from Eqs. (6), (7) and Eq. (17). With the electrical parasitics taken into account, the total circuit model can be obtained, as shown in Fig. 1. For an SOA integrated with an SGDBR laser, the impact of the SGDBR laser on the SOA section is represented by the resistance R_{in} and the wavelength dependence of the circuit parameters. i is the small-signal current injected into the SOA section. C_p, L_p and R_p represent the package parasitics, and C_s and R_s characterize the chip parasitics. C_t is the sum of the space-charge capacitance of the heterojunction C_{sc} and the diffusion capacitance C_d. The resistances R_1, R_2 and R_{in} cause the damping of the electro-optical resonance. The spatially-averaged small-signal photon storage is modeled by the in-
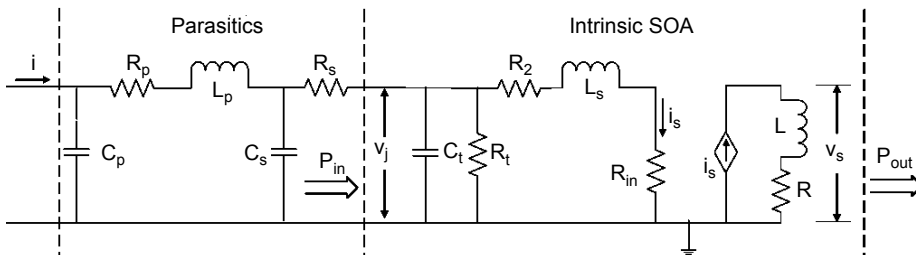

Fig. 1. Small-signal equivalent circuit model of an SOA.

ductance L_S. The traveling-wave effect in the cavity of the SOA section can be represented by R and L. The output small-signal photon density is represented by v_s.

3. Parameters extraction

All the circuit parameters in Fig. 1 can be extracted by fitting the circuit model with the measured S-parameters of an SOA integrated with an SGDBR laser. The device used under our test has been reported with quasi-continuous wavelength coverage over 35 nm and side mode suppression ratio (SMSR) of more than 30 dB for all selected wavelength channels [8]. The experimental setup for the measurement of the S-parameters is illustrated in Fig. 2. The gain section and tuning sections of the device are driven by low noise and high stability current drivers to keep the SGDBR laser working at a certain wavelength. The SOA section is biased through a wide bandwidth bias tee, while a thermoelectric cooler (TEC) controller is introduced to obtain a precise setting and stabilization of the lasing wavelength. The output modulated optical signal of the device is routed to the wide bandwidth optical receiver unit of the network analyzer, which can provide both the reflection response S_{11} (when configured for electrical measurement) and the IM response S_{21} (when configured for electro-optical measurement). The optical receiver response can be calibrated before measurement [9].

When the SOA section is biased at high current above transparency, the space--charge capacitance of heterojunction has a small impedance and small junction dynamic resistance. In this case, the intrinsic part of the SOA section can be modeled
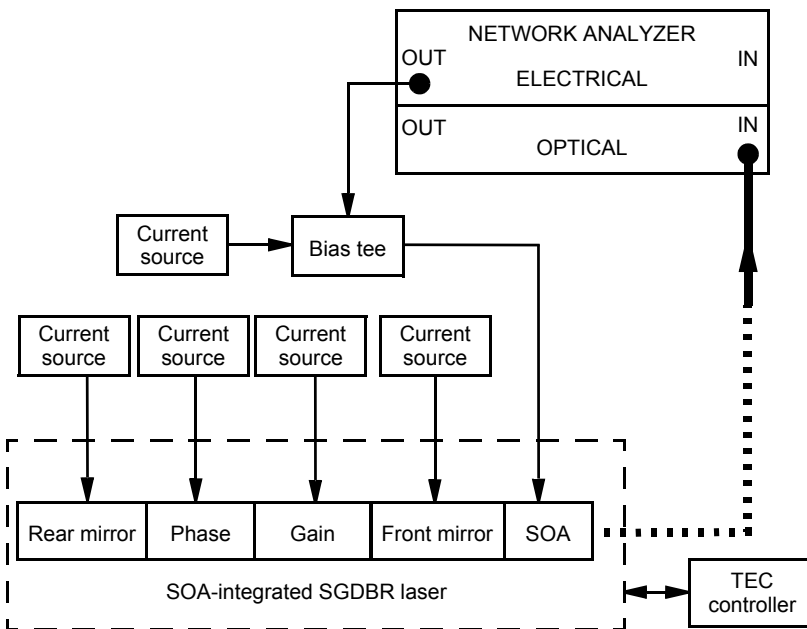

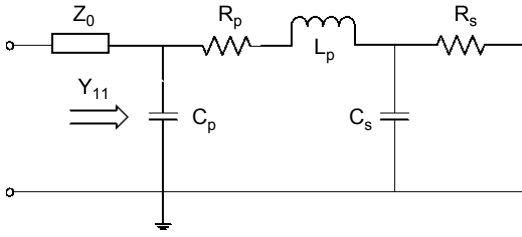Fig. 2. Microwave measurement setup for the SOA section.

Fig. 3. Simplified small-signal equivalent circuit model of the SOA section biased above transparency.

by using a short circuit. So, the small-signal equivalent circuit model can be simplified as shown in Fig. 3, and the parasitic parameters can be regarded invariable for different bias currents [10]. For this situation, the microwave reflection coefficient S_{11} of the input port is entirely determined by the parasitic elements and can be related to the input admittance Y_{11} by [11]

$$S_{11} = \frac{Z_0 Y_{11} - 1}{Z_0 Y_{11} + 1} \tag{19}$$

where Z_0, usually assumed as 50 Ω, is the characteristic impedance of the transmission line between the network analyzer and the SOA section under test. From Fig. 3, we can obtain the expression of Y_{11} as

$$Y_{11} = \frac{1 + j\omega R_s C_s}{R_p + R_s - \omega^2 R_s C_s L_p + j\omega(R_p R_s C_s + L_p)} + j\omega C_p \tag{20}$$

The five parasitic parameters are extracted by fitting the S_{11} converted from the complex admittance of the simplified SOA-section circuit model by Eqs. (19) and (20) with the measured data. Since the parasitic parameters are determined by
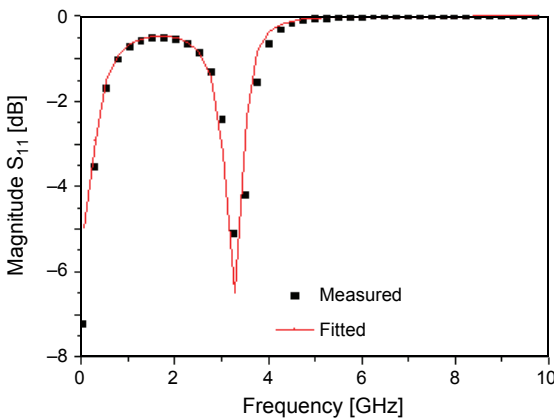

Fig. 4. Measured and fitted S_{11} of the SOA section.

T a b l e 1. Extracted values of the parasitic parameters.

Parameters	Values
C_p [pF]	12.58
L_p [nH]	0.29
R_p [Ω]	0.47
C_s [pF]	21.26
R_s [Ω]	8.62

the electrical characteristics of the SOA section, they are independent of the wavelength of the input optical signal. The measured and fitted S_{11} of the SOA section are presented in Fig. 4, and the extracted values of the parasitic parameters are given in Table 1.

The IM response S_{21} of the SOA section is determined by both the photon response and the effect of the parasitic elements. The expression of S_{21} is as follows:

$$|S_{21}|^2 = \left|\frac{p_o}{p_i}\right| = \left|\frac{Av_s}{Z_0 \, i^2}\right| = \left|A \, \frac{j\omega L + R}{\sqrt{p_i \, Z_0}} \, \frac{i_s}{i}\right| \tag{21}$$

where p_i is the transmitted radio frequency (RF) power of the network analyzer and set at –10 dBm during the RF measuring process. p_o is the small-signal output power of the SOA section. The coefficient A relates p_o to the small-signal photon density s'. As described in [10], the small-signal current transformation function i_s/i can be expressed as

$$\frac{i_s}{i} = \frac{Z_1 Z_3}{R_s Z_2} \, \frac{R_1}{R_1 + R_2 + R_{\text{in}} - \omega^2 L_s R_1 C_t + j\omega\left[L_s + R_1(R_2 + R_{\text{in}})C_t\right]} \tag{22}$$

where

$$Z_1 = \frac{R_s}{1 + j\omega R_s C_s} \tag{23a}$$

$$Z_2 = R_p + j\omega L_p + Z_1 \tag{23b}$$

$$Z_3 = \frac{Z_2}{1 + j\omega Z_2 C_p} + Z_0 \tag{23c}$$

Substituting Eqs. (22), (23) in Eq. (21) and fitting Eq. (21) with the measured S_{21}, we can extract all the intrinsic circuit parameters. To avoid the numerical overflow problem that occurs in the general circuit simulator, the output voltage v_s is normalized by the static photon density S_0'. From Eqs. (8) and (18), we can see that all the intrinsic
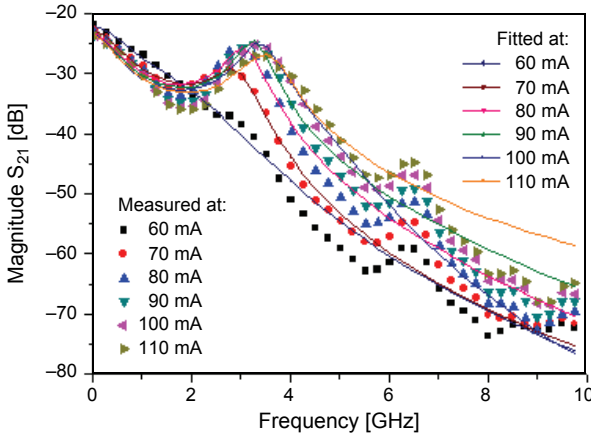
Fig. 5. Measured and fitted IM response of the SOA section for different bias currents (operating wavelength of the SGDBR laser is set at 1541.35 nm).

circuit parameters are dependent on the dc components of the photon and carrier density, which are determined by the static bias current of the SOA section with Eqs. (1) and (2). Figure 5 gives the measured and fitted S_{21} for different bias currents on the SOA section, where the operating wavelength is set at 1541.35 nm. The extracted intrinsic circuit parameters corresponding to Fig. 5 are shown in Tab. 2.

T a b l e 2. Extracted values of the intrinsic parameters for different bias currents of the SOA section. Operating wavelength of the integrated SGDBR laser is set at 1541.35 nm, with the measured parameters: $w = 2.2$ μm, $d = 90$ nm, $l = 600$ μm, $\Gamma = 0.1$, $n_g = 3.6$ (n_g is the group refractive index of the active layer).

Parameters	Bias currents					
	60 mA	70 mA	80 mA	90 mA	100 mA	110 mA
S_0' [m^{-3}]	1.8×10^{22}	2.19×10^{22}	2.67×10^{22}	3.01×10^{22}	3.33×10^{22}	3.62×10^{22}
C_t [pF]	26.8	961.19	875.47	997.47	966.47	998.7
R_1 [Ω]	0.16	3.86	4.67	5.43	5.1	4.55
$R_2 + R_{in}$ [Ω]	13.83	11.88	13.68	12.62	12.17	13.55
L_s [pH]	704.61	1.49×10^3	298.76	17.45×10^{-3}	21.26×10^{-3}	73.76
L [nH]	0.53	0.9	0.79	0.65	0.52	0.44
R [mΩ]	7.13×10^3	181.68	77.98	30.13	58.29	100.53

In our model, the optical gain provided by the SOA section is characterized by the intrinsic circuit parameters. As described in [12], the single-pass gain of the SOA section is a function of the wavelength of the input signal. This feature will lead to the wavelength dependence of the intrinsic circuit parameters. Furthermore, due to the nonuniformity of the output optical power for different wavelength channels [8], the wavelength change of the integrated SGDBR laser can also cause the variation
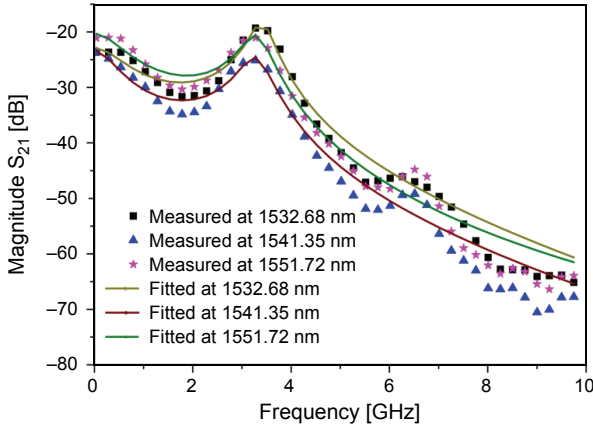
Fig. 6. Measured and fitted IM response of the SOA section for different operating wavelengths (dc bias current of the SOA section is set at 90 mA).

T a b l e 3. Extracted values of the intrinsic parameters for different operating wavelengths. $\lambda_1 =$ = 1532.68 nm, λ_2 = 1541.35 nm, λ_3 = 1551.72 nm, the SOA section is biased at 90 mA, with the measured parameters: w = 2.2 μm, d = 90 nm, l = 600 μm, Γ = 0.1, n_g = 3.6.

Parameters	Operating wavelengths		
	λ_1 = 1532.68 nm	λ_2 = 1541.35 nm	λ_3 = 1551.72 nm
S_0' [m^{-3}]	2.56×10^{22}	3.01×10^{22}	2.9×10^{22}
C_t [pF]	385.06	997.47	995.78
R_1 [Ω]	0.71	5.43	2.76
$R_2 + R_{in}$ [Ω]	4.73	12.62	7.05
L_s [pH]	0.74	17.45×10^{-3}	71.58
L [nH]	0.44	0.65	0.89
R [mΩ]	307	30.13	139.62

of the input power of the SOA section, which will have an impact on the intrinsic circuit parameters by changing the dc components of the photon and carrier density mentioned above. The wavelength dependence of the intrinsic circuit model can be seen in Fig. 6, which gives the measured and fitted S_{21} curves for different operating wavelengths at the bias of 90 mA on the SOA section. The extracted intrinsic circuit parameters corresponding to Fig. 6 are listed in Tab. 3.

4. Optical frequency chirp analysis

A phase modulation will take place when the injected current of the SOA section is amplitude modulated due to the complex susceptibility of the gain medium in the SOA [13, 14]. The small-signal circuit model can be used to determine the fre-

quency modulation (FM) response of the SOA section. The optical frequency shift at the output facet of the SOA section can be expressed as [15]

$$\Delta \nu(t) \; = \; \frac{\alpha}{4\pi} \frac{\mathrm{d} \ln\left[P_o(t) \right]}{\mathrm{d}\, t} \tag{24}$$

where α is the linewidth enhancement factor and $P_o(t)$ is the output optical power of the SOA section and can be obtained by [7]

$$P_o(t) \; = \; \frac{v_g w d h \nu(t) S(l,\, t)}{\Gamma} \tag{25}$$

where h is the Planck constant, v_g is the group velocity at the output facet of the SOA section, and $\nu(t)$ is the optical frequency of the output signal. We split $\nu(t)$ into dc and ac components as

$$\nu(t) \; = \; \nu_0 + \nu_1 \exp(\, j\omega t) \tag{26a}$$

$$\Delta \nu(t) \; = \; \nu_1 \exp(\, j\omega t) \tag{26b}$$

where ν_1 is the small-signal FM component at the output facet of the SOA section. With Eq. (14), Eqs. (25), (26) substituted in Eq. (24), and Eq. (24) can be linearized to

$$\nu_1 \; = \; \frac{\nu_0}{S_0'} \frac{j\omega}{\dfrac{4\pi}{\alpha}\nu_0 - j\omega} s' \tag{27}$$

and

$$\left| \nu_1 \right| \; = \; \frac{\nu_0}{S_0'} \frac{\omega}{\sqrt{\left(\dfrac{4\pi}{\alpha}\nu_0 \right)^2 + \omega^2}} |s'| \approx \frac{\alpha}{4\pi}\, \omega \left| \frac{v_s}{S_0'} \right| \quad \left(\omega \ll \frac{4\pi}{\alpha}\nu_0 \right) \tag{28}$$

Therefore, the current i_1 through the capacitance C_{FM} in the circuit model shown in Fig. 7 can be used as a quantitative analog of the optical frequency chirp term ν_1. Since α has a value of approximately 5 in InGaAsP [16], the value of the capacitance C_{FM} can be considered to be as about 0.4 F. As described in [1], the optical frequency chirp caused by the current modulation of the SOA section is dependent on the amplifier bias, which can be divided into two cases. The measured *P–I* curve of the SOA section for the signal wavelength of 1541.35 nm is given in Fig. 8. When the bias current is less than 90 mA, the gain saturation of the SOA section can be neglected to assume a simple case. In this case, the strength of the frequency modulation is greater for higher amplifier bias. This point can be confirmed by

▲
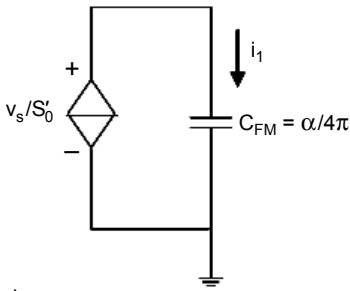
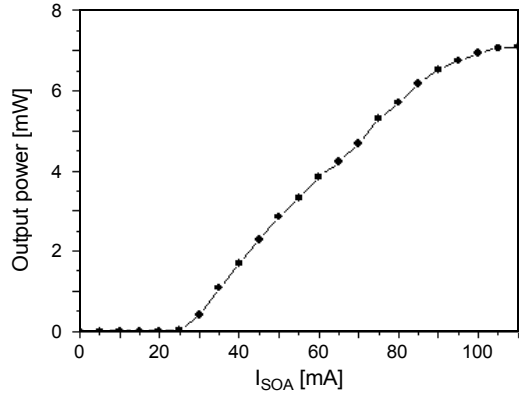Fig. 7. Small-signal equivalent circuit model for FM of the SOA section.

Fig. 8. Measured *P–I* curve of the SOA section (operating wavelength of the integrated SGDBR laser is set at 1541.35 nm).

the calculated results from our small-signal circuit model, as shown in Fig. 9. Different from the IM response in Fig. 6, which has the conventional low-pass shape with a resonance peak, the FM response is depressed sharply below a low-frequency turn point. It has a resonance peak at approximately the same frequency as the IM response. As shown in Fig. 8, when the amplifier bias is higher than 90 mA, the gain saturation becomes serious and cannot be neglected. According to the measured results provided in [1], the occurrence of the amplifier gain saturation will depress frequency modulation, which is consistent with our simulation results shown in Fig. 9. To clearly demonstrate the chirp characteristics, a repeated 2-bit patterned sequence '10' of
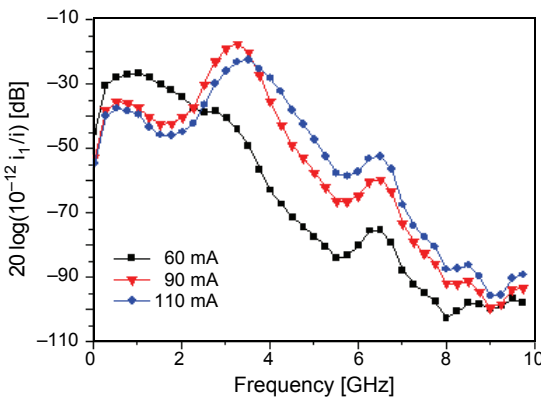

Fig. 9. Calculated FM responses for different bias currents of the SOA section (operating wavelength of the integrated SGDBR laser is set at 1541.35 nm).
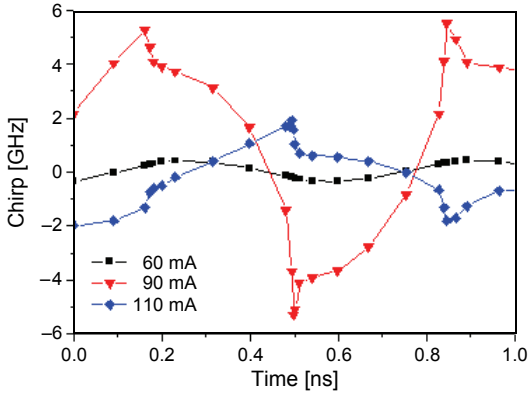
Fig. 10. Simulated output chirp for different bias currents of the SOA section in time domain (operating wavelength of the integrated SGDBR laser is set at 1541.35 nm).

3 Gbit/s has been used to simulate the current modulation of the SOA section. The peak–peak current of 20 mA is selected to avoid the deviation from our small--signal model. The simulation results of the output frequency chirp in time domain are given in Fig. 10, where the maximum chirp of several GHz can be observed, which is comparable to the measured results for the direct modulation of the SGDBR laser [17].

5. Conclusions

In this paper, we have proposed a small-signal equivalent circuit model for an SOA, which is monolithically integrated with an SGDBR laser. In this model, the interaction between the photon density and injected current of the SOA section, including the traveling-wave effect in the SOA, is taken into account. The parasitic circuit parameters are extracted separately from the intrinsic part with some simplifications. All the circuit parameters are obtained by fitting the circuit model with the experimentally measured microwave *S*-parameters of the total device. The intrinsic parameters of our circuit model are dependent on the static bias current of the SOA section and the operating wavelength of the integrated SGDBR laser. The extraction of parameters has been performed on different conditions and all the fitted results agree well with the measured data. The optical frequency chirp caused by the current modulation of the amplifier has been analyzed with our small-signal circuit model and the simulation results are consistent with those measured earlier.

References

[1] San-Liang Lee, Heimbuch M.E., Cohen D.A., Coldren L.A., DenBaars S.P., *Integration of semiconductor laser amplifiers with sampled grating tunable lasers for WDM applications*, IEEE Journal of Selected Topics in Quantum Electronics **3**(2), 1997, pp. 615–627.

[2] Ward A.J., Robbins D.J., Busico G., Barton E., Ponnampalam L., Duck J.P., Whitbread N.D., Williams P.J., Reid D.C.J., Carter A.C., Wale M.J., *Widely tunable DS-DBR laser with monolithically integrated SOA: Design and performance*, IEEE Journal of Selected Topics in Quantum Electronics **11**(1), 2005, pp. 149–156.

[3] Nielsen M.L., Sudo S., Mizutani K., Okamoto T., Tsuruoka K., Sato K., Kudo K., *Integration of functional SOA on the gain chip of an external cavity wavelength tunable laser using etched mirror technology*, IEEE Journal of Selected Topics in Quantum Electronics **13**(5), 2007, pp. 1104–1111.

[4] Hansen P.B., Raybon G., Wiesenfeld J.M., Burrus C.A., Logan R.A., Tanbun-Ek T., Temkin H., *Optical demultiplexing at 6 Gb/s using a semiconductor laser amplifier as an optical gate*, IEEE Photonics Technology Letters **3**(11), 1991, pp. 1018–1020.

[5] Mork J., Mecozzi A., Eisenstein G., *The modulation response of a semiconductor laser amplifier*, IEEE Journal of Selected Topics in Quantum Electronics **5**(3), 1999, pp. 851–860.

[6] Tucker R.S., Pope D.J., *Microwave circuit models of semiconductor injection lasers*, IEEE Transactions on Microwave Theory and Techniques **31**(3), 1983, pp. 289–294.

[7] Chu C.Y.J., Ghafouri-Shiraz H., *Analysis of gain and saturation characteristics of a semiconductor laser optical amplifier using transfer matrices*, Journal of Lightwave Technology **12** (8), 1994, pp. 1378–1386.

[8] Hui Lv, Tan Shu, Yonglin Yu, Dexiu Huang, Lei Dong, Ruikang Zhang, *Fast power control and wavelength switching in a tunable SOA-Integrated SGDBR laser*, in 14th OptoElectronics and Communications Conference (OECC 2009), 2009, paper ThPD4.

[9] Hale P.D., Williams D.F., *Calibrated measurement of optoelectronic frequency response*, IEEE Transactions on Microwave Theory and Techniques **51**(4), 2003, pp. 1422–1429.

[10] Jianjun Gao, Xiuping Li, Flucke J., Boeck G., *Direct parameter-extraction method for laser diode rate-equation model*, Journal of Lightwave Technology **22**(6), 2004, pp. 1604–1609.

[11] Yikai Su, Simsarian J.E., Liming Zhang, *Improving the switching performance of a wavelength-tunable laser transmitter using a simple and effective driver circuit*, IEEE Photonics Technology Letters **16**(9), 2004, pp. 2132–2134.

[12] Durhuus T., Mikkelsen B., Stubkjaer K.E., *Detailed dynamic model for semiconductor optical amplifiers and their crosstalk and intermodulation distortion*, Journal of Lightwave Technology **10**(8), 1992, pp. 1056–1065.

[13] Harder C., Vahala K., Yariv A., *Measurement of the linewidth enhancement factor α of semconductor lasers*, Applied Physics Letters **42**(4), 1983, pp. 328–330.

[14] Arakawa Y., Yariv A., *Fermi energy dependence of linewidth enhancement factor of GaAlAs buried heterostructure lasers*, Applied Physics Letters **47**(9), 1985, pp. 905–907.

[15] Coldren L.A., Corzine S.W., *Diode Lasers and Photonic Integrated Circuits*, Wiley, 1995.

[16] Tucker R., *High-speed modulation of semiconductor lasers*, Journal of Lightwave Technology **3**(6), 1985, pp. 1180–1192.

[17] Maher R., Kai Shi, Anandarajah P.M., Kaszubowska A., Barry L.P., Yonglin Yu, *Novel frequency chirp compensation scheme for directly modulated SG DBR tunable lasers*, IEEE Photonics Technology Letters **21**(5), 2009, pp. 340–342.